Int. J. Solids Structures, 1968, Vol. 4, pp. 1107 to 1123. Pergamon Press. Printed in Great Britain

IMPACTS OF TWO-AXLE SYSTEM TRAVERSING A BEAM

L. FRÝBA

Research Institute of Transport, Prague, Czechoslovakia

Abstract—The problem of vibrations of simple beam carrying an elastic layer and with irregularities on the travel surface is studied. The vibrations are forced by impacts of a moving system of four degrees of freedom, which is an idealization of a two-axle vehicle moving along a bridge. The mathematical formulation of the problem is covered by a system of five differential equations with variable coefficients, which is solved numerically using the computer. The analysis of the effect of some dimensionless parameters gives several important results, e.g. the greatest dynamic effects due to an isolated unevenness arise at the low movement velocity.

NOTATION

$a_i, \bar{a}_i$	depth of an unevenness
$b_i, \bar{b}_i$	length of an unevenness
c	velocity of the movement
d	axle base parameter (26), $d_i = D_i/D$
$f_{(j)}$	jth natural frequency of the beam (31)
f_i	frequency of unsprung mass (33)
f_{3i}	frequency of sprung mass (32)
g	gravitational constant
h, h_1, h_2	integration steps
$j = 1, 2, 3, \ldots$	or $j = 1, 2, 3, \ldots, s$
l	span of the beam
m	mass of the whole vehicle
m_i	unsprung mass of the vehicle
m_3	sprung mass of the vehicle
$q_{(j)}(\tau)$	dimensionless generalized time-coordinate of the beam
$r_i(\xi_i), \bar{r}_i(x_i)$	coordinates of irregularities on travel surface
s	maximum value of j
t	time coordinate
$u_i(t)$	approach of two bodies during the impact
$v(\xi, \tau), \bar{v}(x, t)$	deflection of the beam
$v_i(\tau), \bar{v}_i(t)$	vertical displacement of mass m_i
$v_3(\tau), \bar{v}_3(t)$	vertical displacement of sprung mass m_3
$v_{3i}(\tau), \bar{v}_{3i}(t)$	vertical displacement of sprung mass over the ith axle
v_0	deflection of the beam-center loaded at $x = l/2$ by the force $P/2$, (30)
x	length coordinate
x_i	coordinates of contact points (1)
$z_i(\tau)$	dimensionless quantity (46)
$A_i, \bar{A}_i$	distance between two points of unevenness or circumference of a wheel
$B_i, \bar{B}_i$	distance of the first unevenness from $x = 0$
C_i	spring constant of the vehicle
C_{bi}	viscous damping coefficient of vehicle springs
D, D_i	axle base, distance as in Figs. 1 and 2
EJ	bending modulus of the beam
$G = \mu g l$	weight total of the beam
I	polar moment of inertia of sprung mass about centroid O, see Fig. 1 and 2
K_i	spring constant of tires or of springs substituting the roadway under the ith axle
$M(\xi, \tau), \bar{M}(x, t)$	bending moment of the beam
M_0	bending moment at the beam-centre loaded at $x = l/2$ by the force $P/2$, see equation (54)

$M_{Ri}(\xi, \tau)$	dimensionless bending moment caused by the load $R_i(\tau)$ placed in ξ_i, see equation (55)
$M_\mu(\xi, \tau)$	dimensionless bending moment caused by inertia forces $-\mu\bar{v}(x, t)$, see equation (56)
N	intermediate results printed after each Nth step, they are not printed for $N = 0$
$P = mg = P_1 + P_2 + P_3$	weight total of vehicle
$P_i = m_i g$	static unsprung weight of the vehicle
$P_3 = m_3 g$	static sprung weight of the vehicle
$P_{3i} = P_3 D_{\bar{i}}/D$	static sprung weight per ith axle
Q_i	dimensionless static load, see equation (47)
$R_i(\tau), \bar{R}_i(t)$	moving dynamic contact force between ith axle and the beam, see equations (10), (15), (48)
$Z_i(t)$	force in spring C_i
$Z_{bi}(t)$	damping force in spring C_i
α	velocity parameter (19)
β_i	sprung frequency parameter (20)
γ_i	unsprung frequency parameter (21)
$\delta(\xi), \delta(x)$	Dirac-delta function
$\varepsilon_i, \bar{\varepsilon}_i$	function (12)
η	auxiliary length coordinate
ϑ, ϑ_i	logarithmic damping decrement in the beam and in the spring C_i, respectively
$\varkappa$	mass parameter (16)
$\varkappa_i$	unsprung mass parameter (17)
λ	rotatory parameter (18)
μ	constant mass per unit length of the beam
ξ	dimensionless length coordinate (34)
ξ_i	dimensionless coordinate of contact point (44)
τ	dimensionless time coordinate (34)
$\varphi(\tau), \bar{\varphi}(t)$	rotation of the sprung mass
ω_b	circular damping frequency of the beam

Subscripts

$i = 1, 2$	right or left axle, respectively (unsprung mass)
$\bar{i} = 1$ for $i = 2$, $\bar{i} = 2$ for $i = 1$	
0	initial
3	sprung mass
b	damping

Superscripts

$'$, iv	differentiation with respect to x or ξ
$\cdot$, $\ddot{}$	differentiation with respect to t or τ
$-$	dimensional form of a quantity

1. INTRODUCTION

THE paper deals with the vibration of a beam subjected to the dynamic action of moving loads. This classical problem has been solved since the 19th century in connection with the development of modern transport.

The first authors, R. Willis, G. G. Stokes and H. Zimmermann, see [1], assumed a single mass moving along a massless simply supported beam. A. N. Krylov and S. P. Timoshenko, see [1], considered the opposite case, i.e. the movement of a force along a mass-beam. The general case considering both the mass of the beam and that of the moving load was solved much later by many authors; excellent applications of this theory to the vibration of railway bridges are due to Inglis [2] and Koloušek [3].

The more complicated problem of a sprung mass traversing a beam has been solved recently by Hillerborg [4], Biggs *et al.* [5] and Tung *et al.* [6]. The author of the present paper considered in [7] a two-mass system (sprung and unsprung mass) moving along a beam, the surface of which is covered with an elastic layer of variable stiffness and with

irregularities on the travel surface. In practice this idealization is convenient for large span bridges but it is not satisfactory when the span is short. In the latter case the axle base is comparable with span length of the bridge.

The dynamic response of a beam traversed by two-axle loads has been solved by Wen [8] whose solution supposes permanent contact between the wheels and the roadway. However, with regard to the track or wheel irregularities the case of loss of contact can very easily occur. For that reason the present paper brings the solution of a most general case when also impacts* between the moving system and the beam may occur. The analysis is suitable for the dynamic calculation of both highway and railway bridges especially of short span.

2. THEORETICAL SOLUTION

2.1 *Formulation of problem*

The mathematical model of the system to be studied is shown schematically in Fig. 1.

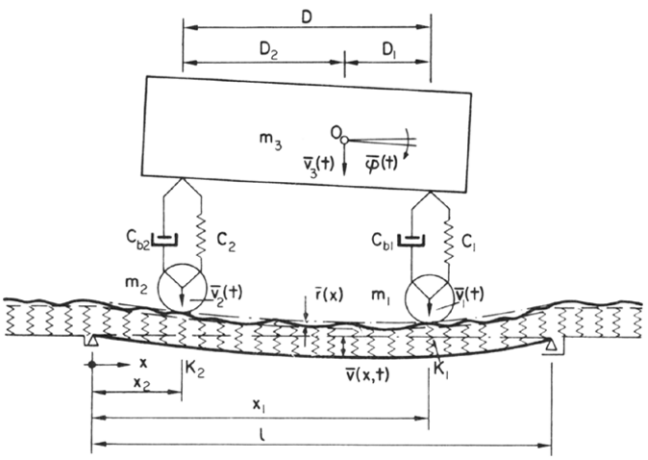

FIG. 1. Model of a beam with an elastic layer and with irregularities; beam subjected to the action of a moving four-degrees-of-freedom system.

We shall consider a uniform beam of length l, simply supported, damped proportionally to the velocity of vibrations and described by the Bernoulli–Euler beam-model. The moving vehicle is considered as a four-degrees of freedom system with two unsprung masses m_i, $i = 1, 2$, and with a sprung mass m_3, which besides the vertical movement is also capable of rotation. The linear springs possess the constants C_i and the viscous damping coefficients C_{bi}.

The roadway of railway bridges is idealized by an elastic layer with spring constants K_i under the ith axle, see Fig. 1. The constants K_i applicable for the calculation of highway bridges represent the spring constants of tires, see Fig. 2. Irregularities of the roadway travel surface $\bar{r}_i(x_i)$ which may be different under each axle will be considered. In such a

* The impact is here defined as a collision of two moving solids.

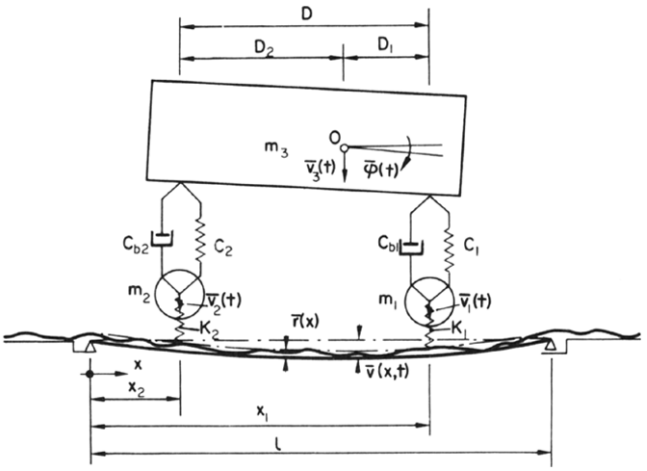

FIG. 2. Model of a beam with irregularities loaded by a moving system of four degrees of freedom.

manner various types of irregularities of track or wheels (e.g. flat wheels, an isolated unevenness of roadway, undulated surface of the roadway etc.) may be considered, see Fig. 3.

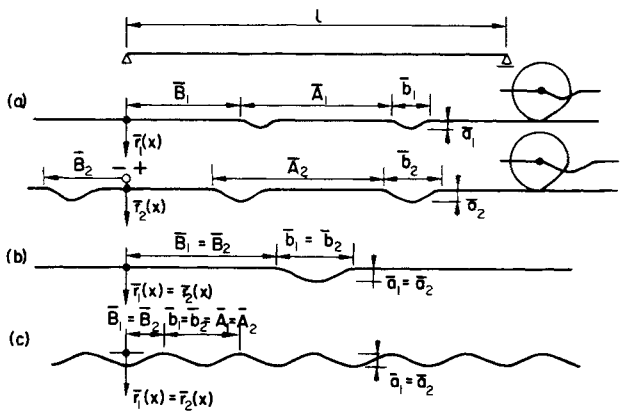

FIG. 3. Irregularities on the travel surface: (a) effect of flat wheels, (b) isolated unevenness on the roadway surface, (c) undulated surface of the roadway.

The vehicle is assumed as moving from left to right with constant velocity c, so that the coordinates of the contact points are

$$x_1 = ct, \qquad x_2 = ct - D \tag{1}$$

where D is the axle base, see Figs. 1 and 2. The beam is supposed to be at rest when the vehicle (which can vibrate in this moment) starts to move across it.

Following the assumptions mentioned above the problem may be covered by a system of five linear differential equations with variable coefficients, which describe the rotation and vertical movement of the sprung mass, the vertical movements of unsprung masses

and the bending vibration of the beam, respectively:

$$-I\ddot{\bar{\varphi}}(t)+\sum_{i=1}^{2}(-1)^i D_i[Z_i(t)+Z_{bi}(t)]=0, \tag{2}$$

$$-m_3\ddot{\bar{v}}_3(t)-\sum_{i=1}^{2}[Z_i(t)+Z_{bi}(t)]=0, \tag{3}$$

$$P_i+P_{3i}-m_i\ddot{\bar{v}}_i(t)+Z_i(t)+Z_{bi}(t)-\bar{R}_i(t)=0; \qquad i=1,2, \tag{4),(5}$$

$$EJ\bar{v}^{iv}(x,t)+\mu\ddot{\bar{v}}(x,t)+2\mu\omega_b\dot{\bar{v}}(x,t)=\sum_{i=1}^{2}\bar{\varepsilon}_i\bar{\delta}(x-x_i)\bar{R}_i(t). \tag{6}$$

The following notations were used in equations (2)–(6):

$\bar{v}(x,t)$ the deflection of the beam using static deflection by the beam mass μ as datum
$\bar{v}_i(t)$ vertical displacement of mass m_i measured from the position when the springs K_i are undeformed
$\bar{v}_3(t)$ vertical displacement of sprung mass m_3 measured from the position before entering the beam (springs C_i are deformed by sprung mass so that $P_3=\sum_{i=1}^{2}C_i v_{3i0}$, see equation (7))
$\bar{\varphi}(t)$ clockwise rotation of sprung mass measured from the horizontal direction

$$\bar{v}_{3i}(t)=\bar{v}_3(t)-(-1)^i D_i\bar{\varphi}(t); \qquad i=1,2 \tag{7}$$

vertical displacement of the sprung mass over the ith axle,

$$Z_i(t)=C_i[\bar{v}_{3i}(t)-\bar{v}_i(t)]; \qquad i=1,2 \tag{8}$$

force in spring C_i,

$$Z_{bi}(t)=C_{bi}[\dot{\bar{v}}_{3i}(t)-\dot{\bar{v}}_i(t)]; \qquad i=1,2 \tag{9}$$

damping force in spring C_i,

$$\bar{R}_i(t)=K_i u_i(t)\geqq 0; \qquad i=1,2 \tag{10}$$

moving dynamic contact force between the ith axle and the beam where

$$u_i(t)=\bar{v}_i(t)-\bar{\varepsilon}_i\bar{v}(x_i,t)-\bar{r}_i(x_i); \qquad i=1,2 \tag{11}$$

the approach of the ith unsprung mass and the beam,

$$\bar{\varepsilon}_i=\begin{cases}1 \text{ for } 0\leqq x_i\leqq l,\\ 0 \text{ for } x_i<0;\ x_i>l,\end{cases} \qquad i=1,2 \tag{12}$$

$\bar{\delta}(x)$ the Dirac-delta function

The other notations and symbols are explained in the section Notation in alphabetical order.

The boundary conditions of the beam are

$$\bar{v}(0,t)=0, \qquad \bar{v}(l,t)=0, \qquad \bar{v}''(0,t)=0, \qquad \bar{v}''(l,t)=0 \tag{13}$$

and the initial conditions:

$$\begin{aligned}&\bar{v}(x,0)=0, && \dot{\bar{v}}(x,0)=0,\\ &\bar{v}_i(0)=\bar{v}_{i0}, && \dot{\bar{v}}_i(0)=\dot{\bar{v}}_{i0},\ i=1,2\\ &\bar{v}_3(0)=\bar{v}_{30}, && \dot{\bar{v}}_3(0)=\dot{\bar{v}}_{30},\\ &\bar{\varphi}(0)=\bar{\varphi}_0, && \dot{\bar{\varphi}}(0)=\dot{\bar{\varphi}}_0.\end{aligned} \tag{14}$$

The contact force between the two bodies is generally

$$\bar{R}_i(t)=k_2 u_i^{\frac{3}{2}}(t) \tag{15}$$

following the Hertz's contact law, the constant k_2 see [9], where the approach of two bodies $u_i(t)$ is given by the equation (11). In practical cases it may be sufficient to linearize the relation (15) by the equation (10), see [10]. The equation (10) is an approximate relation for the contact of two bodies and it can be interpreted by introducing the linear springs K_i, see Figs. 1 and 2.

The contact force $\bar{R}_i(t)$ must be positive or zero. If $u_i(t) < 0$ then $\bar{R}_i(t) = 0$ is to be substituted in equations (4)–(6). At this moment the natural vibration of the beam and of the vehicle occurs because both systems lose the contact. In a short time interval, i.e. when again $u_i(t) = 0$, $i = 1, 2$, an impact takes place accompanied by $\bar{R}_i(t) > 0$.

2.2 *Dimensionless parameters*

The problem formulated for calculations using the computer can be described by 30 dimensionless parameters*:

$$\varkappa = P/G, \tag{16}$$

$$\varkappa_i = P_i/P; \qquad i = 1, 2, \tag{17}$$

$$\lambda = I/(mD^2), \tag{18}$$

$$\alpha = c/(2f_{(1)}l), \tag{19}$$

$$\beta_i = f_{3i}/f_{(1)}; \qquad i = 1, 2, \tag{20}$$

$$\gamma_i = f_i/f_{(1)}; \qquad i = 1, 2, \tag{21}$$

$$a_i = \bar{a}_i/v_0; \qquad i = 1, 2, \tag{22}$$

$$b_i = \bar{b}_i/l; \qquad i = 1, 2, \tag{23}$$

$$A_i = \bar{A}_i/l; \qquad i = 1, 2, \tag{24}$$

$$B_i = \bar{B}_i/l; \qquad i = 1, 2, \tag{25}$$

$$d = D/l, \tag{26}$$

$$d_1 = D_1/D, \tag{27}$$

$$\vartheta = \omega_b/f_{(1)}, \tag{28}$$

$$\vartheta_i = C_{bi}/(2mf_{3i}); \quad i = 1, 2. \tag{29}$$

In equations (16)–(29) denotes:

$$v_0 = Pl^3/(96\,EJ) \tag{30}$$

—deflection of the beam at $x = l/2$ if the static concentrated load $P/2$ is acting on the same coordinate, i.e. at $x = l/2$,

$$f_{(j)} = \frac{j^2\pi}{2l^2}\left(\frac{EJ}{\mu}\right)^{\frac{1}{2}}; \qquad j = 1, 2, 3, \ldots \tag{31}$$

* Eight initial conditions (42) except the first two are also numbered among the input parameters for the computer. In addition, five following auxiliary parameters were used: the number of the case, integration steps h_1 and h_2, the number N and the number s which are explained in the following sections. A sample of a set of input parameters is given in Table 1.

—natural frequency of the beam,

$$f_{3i} = \frac{1}{2\pi}\left(\frac{C_i}{m}\right)^{\frac{1}{2}}; \qquad i = 1, 2 \tag{32}$$

—frequency of sprung mass,

$$f_i = \frac{1}{2\pi}\left(\frac{K_i}{m}\right)^{\frac{1}{2}} \tag{33}$$

—frequency of unsprung mass.

The lengths $\bar{a}_i$, $\bar{b}_i$, $\bar{A}_i$, $\bar{B}_i$ are evident from Fig. 3 and explained in the following section. The dimensionless forms of these quantities are a_i, b_i, A_i, B_i, respectively.

2.3 *Transformation of equations into dimensionless form*

There are introduced dimensionless independent variables

$$\xi = x/l, \qquad \tau = ct/l \tag{34}$$

and dependent ones

$$\begin{aligned} v(\xi, \tau) &= \bar{v}(x, t)/v_0, \qquad v_i(\tau) = \bar{v}_i(t)/v_0; \qquad i = 1, 2, \\ v_3(\tau) &= \bar{v}_3(t)/v_0, \qquad \varphi(\tau) = \bar{\varphi}(t)D/v_0. \end{aligned} \tag{35}$$

Putting (16)–(35), equations (2)–(6) may be written in this form:

$$\ddot{\varphi}(\tau) = \frac{1}{\lambda\alpha^2}\sum_{i=1}^{2}(-1)^i d_i\beta_i[\pi^2\beta_i z_i(\tau) + \vartheta_i\alpha\dot{z}_i(\tau)], \tag{36}$$

$$\ddot{v}_3(\tau) = -\frac{1}{\left(1-\sum_{i=1}^{2}\varkappa_i\right)\alpha^2}\sum_{i=1}^{2}\beta_i[\pi^2\beta_i z_i(\tau) + \vartheta_i\alpha\dot{z}_i(\tau)], \tag{37}$$

$$\ddot{v}_i(\tau) = \frac{48}{\pi^2\varkappa_i\varkappa\alpha^2}\left[2Q_i + \frac{\pi^4}{48}\varkappa\beta_i^2 z_i(\tau) + \frac{\pi^2}{48}\vartheta_i\beta_i\varkappa\alpha\dot{z}_i(\tau) - R_i(\tau)\right]; \qquad i = 1, 2, \tag{38), (39}$$

$$v^{\mathrm{iv}}(\xi, \tau) + \pi^2\alpha^2\ddot{v}(\xi, \tau) + \pi^2\vartheta\alpha\dot{v}(\xi, \tau) = 48\sum_{i=1}^{2}\varepsilon_i\delta(\xi - \xi_i)R_i(\tau). \tag{40}$$

The boundary conditions are now

$$\begin{aligned} v(0, \tau) &= 0, \qquad v(1, \tau) = 0, \\ v''(0, \tau) &= 0, \qquad v''(1, \tau) = 0 \end{aligned} \tag{41}$$

and the initial conditions:

$$\begin{aligned} v(\xi, 0) &= 0, \qquad \dot{v}(\xi, 0) = 0, \\ v_i(0) &= v_{i0}, \qquad \dot{v}_i(0) = \dot{v}_{i0}; \qquad i = 1, 2 \\ v_3(0) &= v_{30}, \qquad \dot{v}_3(0) = \dot{v}_{30}, \\ \varphi(0) &= \varphi_0, \qquad \dot{\varphi}(0) = \dot{\varphi}_0. \end{aligned} \tag{42}$$

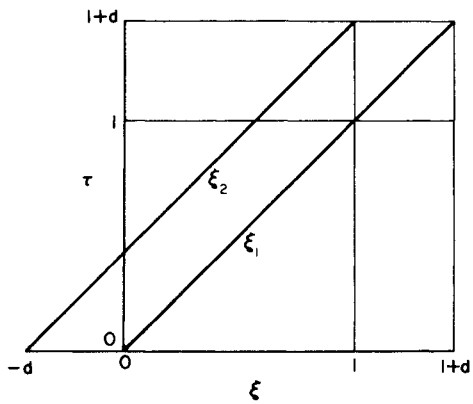

FIG. 4. Interval of integration.

The problem is integrated in the interval, see Fig. 4

$$0 \leqq \xi \leqq 1, \qquad 0 \leqq \tau \leqq 1+d \tag{43}$$

As follows from equation (1), the coordinates of contact points are

$$\xi_1 = ct/l = \tau, \qquad \xi_2 = ct/l - D/l = \tau - d, \tag{44}$$

so that their interval is, see Fig. 4

$$0 \leqq \xi_1 = 1+d, \qquad -d \leqq \xi_2 \leqq 1. \tag{45}$$

In equations (36)–(40) we use now the following notations

$$z_i(\tau) = v_3(\tau) - (-1)^i d_i \varphi(\tau) - v_i(\tau); \qquad i = 1, 2 \tag{46}$$

—for the dimensionless approach of the masses m_i and m_3,

$$Q_i = (P_i + P_{3i})/P = \varkappa_i + d_i\left(1 - \sum_{i=1}^{2} \varkappa_i\right); \qquad i = 1, 2 \tag{47}$$

—for the dimensionless static axle load and

$$R_i(\tau) = 2\bar{R}_i(t)/P = \frac{1}{48}\pi^4 \varkappa \gamma_i^2 [v_i(\tau) - \varepsilon_i v(\xi_i, \tau) - r_i(\xi_i)] \geqq 0, \qquad i = 1, 2 \tag{48}$$

—for the dimensionless dynamic contact force.

ε_i and $\delta(\xi)$ are dimensionless forms of the functions $\tilde{\varepsilon}_i$ and $\tilde{\delta}(x)$, respectively.

The dimensionless coordinates of unevenness of the travel surface following Fig. 3 are:

$$r_i(\xi_i) = \frac{1}{v_0}\bar{r}_i(x_i) = \begin{cases} \dfrac{1}{2}a_i\left[1 - \cos\dfrac{2\pi}{b_i}(\xi_i - k\,A_i - B_i)\right], \\ \\ 0, \qquad i = 1, 2 \end{cases}$$

$$\text{for} \begin{cases} B_i + k\,A_i \leqq \xi_i \leqq B_i + k\,A_i + b_i, \\ B_i + k\,A_i + b_i < \xi_i < B_i + (k+1)A_i, \qquad k = 0, 1, 2, \ldots \end{cases} \tag{49}$$

Several types of irregularities may be expressed by equation (49), see Fig. 3:

(a) The effect of a flat spot on a wheel of a railway car can be assumed as a change of the distance between the centroid of the wheel and the beam. According to the measurement made in [10] the coordinates of this kind of unevenness are equal to equation (49) using the following dimensionless notations: a_i depth; b_i length of the flat spot; A_i wheel circumference; B_i distance of the first impact from $x = 0$, see Fig. 3(a).

(b) An isolated unevenness on the roadway travel surface according to Fig. 3(b) is expressed by equation (49) with $a_1 = a_2$, $b_1 = b_2$, $A_i > 1+d$, $B_1 = B_2$.

(c) The undulated travel surface according to Fig. 3(c): $a_1 = a_2$, $b_1 = b_2$, $A_i = b_i$, $B_1 = B_2$.

2.4 *Rearrangement of equations for numerical solution*

The partial differential equation (40) may be solved by the method of finite Fourier (sinus) integral transformation which is defined by the relations

$$q_{(j)}(\tau) = 2\int_0^1 v(\xi, \tau)\sin j\pi\xi \,\mathrm{d}\xi, \tag{50}$$

$$v(\xi, \tau) = \sum_{j=1}^{\infty} q_{(j)}(\tau)\sin j\pi\xi. \tag{51}$$

where $q_{(j)}(\tau)$ is the dimensionless generalized time-coordinate of the beam deflection. Transforming the equation (40) using (50), then with regard to the boundary conditions (41) we obtain, after some rearrangements, the set of equations

$$\ddot{q}_{(j)}(\tau) = \frac{96}{\pi^2\alpha^2}\sum_{i=1}^{2}\varepsilon_i R_i(\tau)\sin j\pi\xi_i - j^4\frac{\pi^2}{\alpha^2}q_{(j)}(\tau) - \frac{\vartheta}{\alpha}\dot{q}_{(j)}(\tau); \qquad j = 1, 2, 3, \ldots \tag{52}$$

with the initial conditions:

$$q_{(j)}(0) = 0, \qquad \dot{q}_{(j)}(0) = 0. \tag{53}$$

The system (36)–(39) and (52) of differential equations is now suitable for numerical solution.

The calculation of beam-stresses is governed by the magnitude of the bending moment

$$\overline{M}(x, t) = -EJ\,\partial^2\bar{v}(x, t)/\partial x^2.$$

However, the series (51) after its second derivation with respect to ξ becomes of poor convergence,* so that it is more convenient to calculate the dimensionless bending moment in the following way (see [8]):

$$M(\xi, \tau) = \overline{M}(x, t)/M_0 = \sum_{i=1}^{2} M_{Ri}(\xi, \tau) + M_{\mu}(\xi, \tau) \tag{54}$$

where

$$M_0 = Pl/8$$

* The series (51) converges approximately as the series $\sum_{j=1}^{\infty} 1/j^4$ while the series for the bending moment after the second derivation (51) with respect to ξ converges as the series $\sum_{j=1}^{\infty} 1/j^2$. The procedure described below and given by equation (54) improves the calculation of bending moment and the convergence of the series (57) is approximately the same as that one of the series $\sum_{j=1}^{\infty} 1/j^3$.

—is the bending moment at the beam centre loaded in $x = l/2$ by the force $P/2$,

$$M_{Ri}(\xi, \tau) = \begin{cases} \frac{8}{Pl}\frac{1}{l}\bar{\varepsilon}_i\bar{R}_i(t)(l-x_i)x = 4\varepsilon_i R_i(\tau)(1-\xi_i)\xi & \text{for} \quad \xi_i \geqq \xi, \\ \frac{8}{Pl}\frac{1}{l}\bar{\varepsilon}_i\bar{R}_i(t)(l-x)x_i = 4\varepsilon_i R_i(\tau)(1-\xi)\xi_i & \text{for} \quad \xi_i \leqq \xi \end{cases} \tag{55}$$

—is the dimensionless bending moment caused by the load $R_i(\tau)$ placed in ξ_i and

$$M_\mu(\xi, \tau) = \frac{8}{Pl}\left[-\frac{x}{l}\int_0^l \mu\ddot{v}(x, t)(l-x)\,\mathrm{d}x + \int_0^x \mu\ddot{v}(\eta, t)(x-\eta)\,\mathrm{d}\eta\right] \tag{56}$$

—is the dimensionless bending moment caused by the inertia forces $-\mu\ddot{v}(x, t)$.

We substitute the expression (51) into (56) and supposing that the series (51) converges uniformly in $0 \leqq \xi \leqq 1$ the order of integration and summation can be interchanged, so that we obtain

$$M_\mu(\xi, \tau) = -\frac{1}{12}\alpha^2 \sum_{j=1}^{\infty} \frac{1}{j^2}\ddot{q}_{(j)}(\tau)\sin j\pi\xi. \tag{57}$$

The calculation of the bending moment by equations (54)–(57) is convenient because the needed functions $R_i(\tau)$ and $\ddot{q}_{(j)}(\tau)$ must be evaluated anyway if we use the chosen numerical method. The accuracy of calculation is very good, especially at the low movement velocity, i.e. when $M_\mu(\xi, \tau) \ll M_{Ri}(\xi, \tau)$. Using this procedure we develop only a portion of the bending moment caused by the inertia forces in the Fourier series while the effect of the forces $R_i(\tau)$ is calculated directly.

2.5 *Numerical solution*

The initial problem given by the system (36)–(39) and (52) of linear ordinary differential equations of second order with variable coefficients and with the initial conditions (42) and (53) has been solved numerically using the method of Runge–Kutta–Nyström, see [11]. A satisfactory approximation is obtained by taking into account the finite number s of equations (52) (s is one of the given input parameters). The approximate solution of $v(\xi, \tau)$ is then

$$v(\xi, \tau) \approx \sum_{j=1}^{s} q_{(j)}(\tau)\sin j\pi\xi; \qquad j = 1, 2, 3, \ldots, s \tag{58}$$

The computer Ural 2 was used for numerical calculations and the following data are printed after each Nth step: τ, $M(1/2, \tau)$, $v(1/2, \tau)$, $R_1(\tau)$ and $R_2(\tau)$. If $\tau = 1 + d$ the following values are always printed: $\tau[\max M(1/2, \tau)]$, $\max M(1/2, \tau)$, $\tau[\max v(1/2, \tau)]$, $\max v(1/2, \tau)$, $\tau[\max R_i(\tau)]$, $\max R_i(\tau)$, since the positive maxima of data mentioned above are picked out in the course of the calculations.

When h_1 and h_2 are input parameters estimated as in [11] and [7] the integration step is given as follows:

$$h = \begin{cases} h_2 & \text{for} \quad B_i + k\,A_i - h_1 < \xi_i \leqq B_i + k\,A_i + 2\,b_i \\ h_1 & \text{elsewhere}; \qquad i = 1, 2, \qquad k = 0, 1, 2, \ldots \end{cases} \tag{59}$$

h_2 holds true in the vicinity of the impact ($h_2 < h_1$) as we are expecting a great change of dynamic forces here.

The accuracy of calculation using several step length h_1, h_2 and s was verified in the case No. 30 (see Table 1) and the results are given in Table 2. The convergence of the series was very good in this example while in some other cases it was a little poorer.

3. EFFECT OF SOME DIMENSIONLESS PARAMETERS

The effect of some dimensionless parameters was studied using a set of input parameters (case No. 30, Table 1) and changing only one of them in turn keeping the others constant. This case represents the dynamic effect of a two-axle car with a flat spot on the second wheel moving across a short span bridge. A sample of calculations is shown in Fig. 5, and the same case but without any unevenness is represented by Fig. 6.

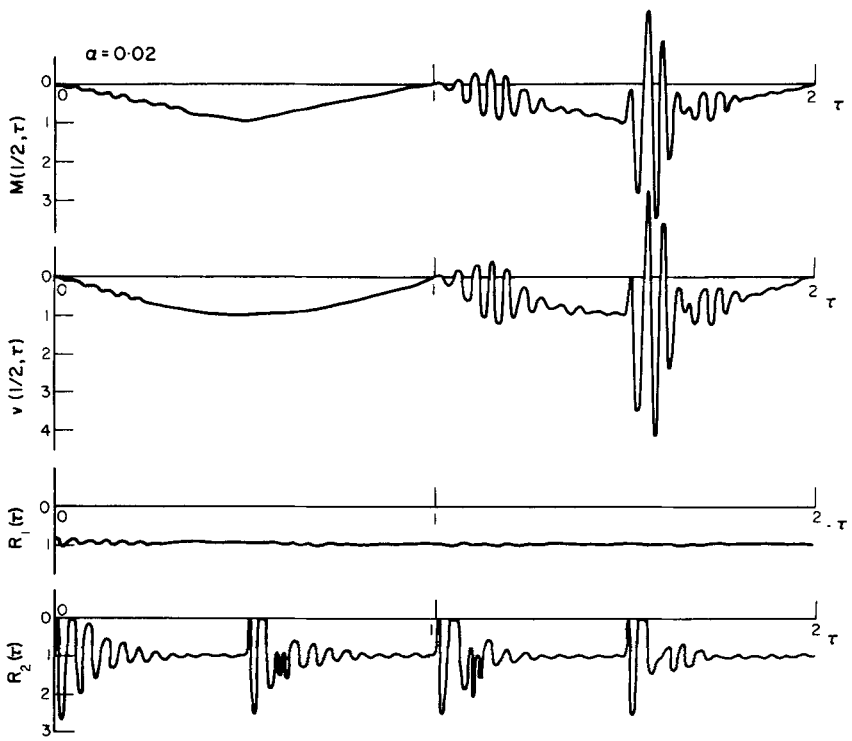

FIG. 5. Time variation of dimensionless bending moment $M(1/2, \tau)$ and deflection $v(1/2, \tau)$ at the beam-centre and of the forces $R_1(\tau)$ and $R_2(\tau)$. Case No. 30, $a_1 = 0$, $a_2 = 20$, $\alpha = 0{\cdot}02$.

In the following figures only the maxima of functions $M(1/2, \tau)$, $v(1/2, \tau)$, $R_1(\tau)$ and $R_2(\tau)$ are plotted.

3.1 *Effect of velocity parameter* α (19)

This is shown in Fig. 7. It is evident that the dynamic effects of impacts of an isolated unevenness (flat spot on a wheel) attain their maximum with low moving velocity. The

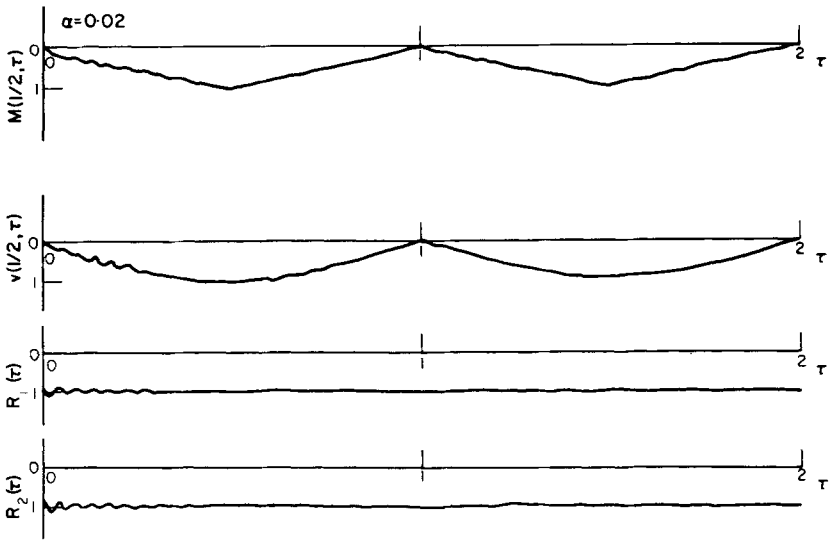

FIG. 6. Time variation of dimensionless bending moment $M(1/2, \tau)$ and deflection $v(1/2, \tau)$ at the beam-centre and of the forces $R_1(\tau)$ and $R_2(\tau)$. Case No. 30, $a_1 = 0$, $a_2 = 0$, $\alpha = 0{\cdot}02$.

axle load max $R_1(\tau)$ of a wheel without any unevenness is almost constant for various α. For comparison Fig. 8 shows the same case but without any unevenness. In this case when no impacts occur the maxima values are much smaller than the maxima in the Fig. 7.

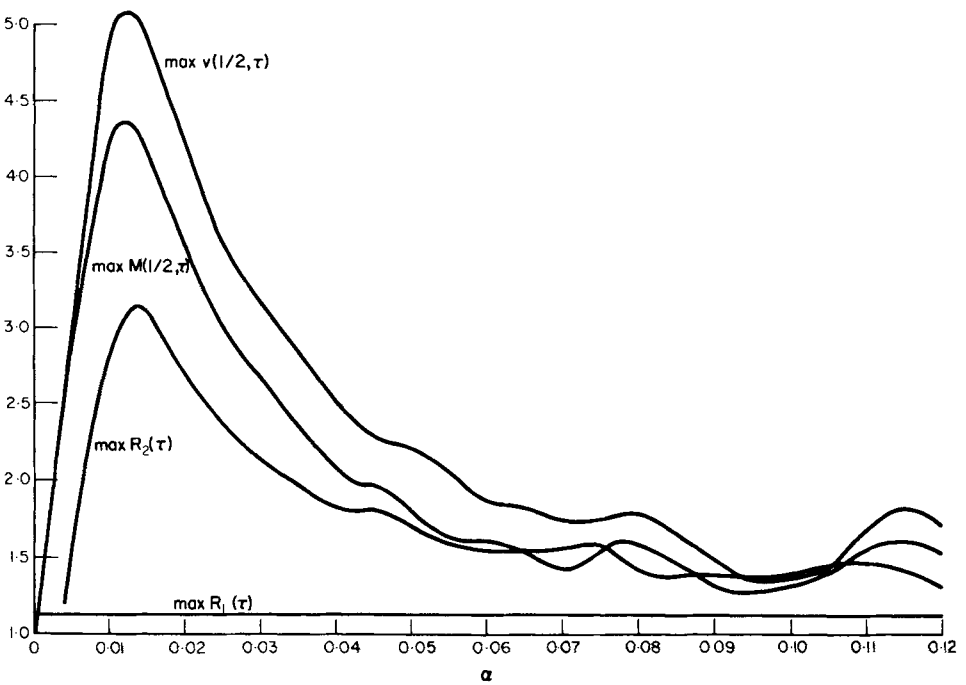

FIG. 7. Effect of the velocity parameter α. Case No. 30, $a_1 = 0$, $a_2 = 20$.

Figure 9 represents the behaviour of impact forces for various α using an enlarged time scale. For the low moving velocity ($\alpha < 0{\cdot}0075$) the contact force keeps positive ($R_2(\tau) > 0$) and no impact occurs. The maximum dynamic effects arise when the contact force decreases

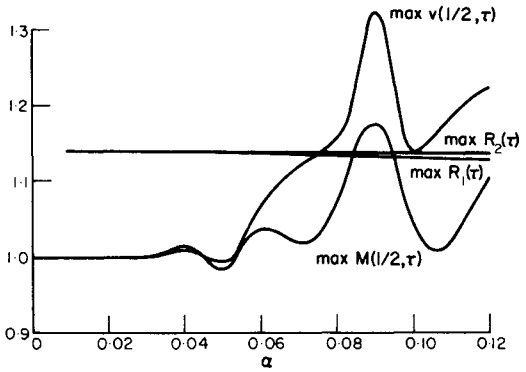

FIG. 8. Effect of the velocity parameter α. Case No. 30, $a_1 = 0$, $a_2 = 0$.

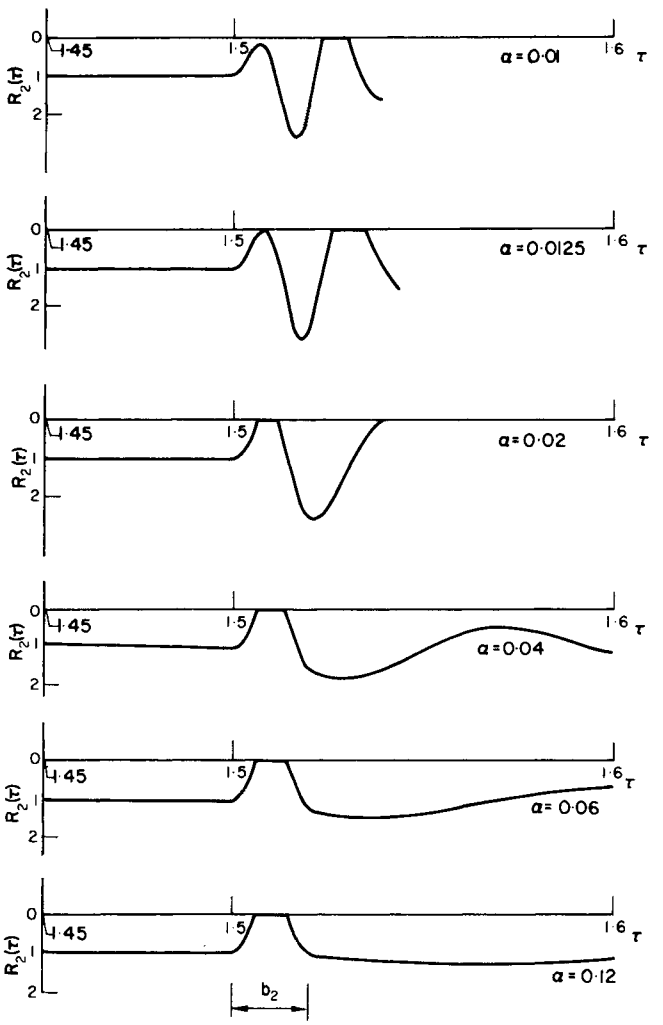

FIG. 9. Time variation of dimensionless force $R_2(\tau)$ near the impact for various α. Case No. 30, $a_1 = 0$, $a_2 = 20$.

to zero at first and then rises ($\alpha \approx 0{\cdot}0125$). The secondary impact occurs after the second unloading. Increasing the velocity ($\alpha \geq 0{\cdot}02$) the wheel loses its contact with the beam just after running on to a flat spot and then one or more impacts occur, see Fig. 9. However, the bending moment and deflection maxima begin decreasing in this case. For $\alpha > 0{\cdot}05$, the unloading and the primary impact always occurs. However, there is no peak characteristic for impact phenomena in this case. The force $R_2(\tau)$ has a similar variation before and after the impact while the bending moment and the deflection of the beam are almost uninfluenced.

3.2 *Effect of parameters* $\varkappa$ (16), β_i (20), γ_i (21) *and* a_2 (22)

These are investigated on Figs. 10–13, respectively, using the set of input parameters No. 30 in Table 1 and keeping other parameters constant.

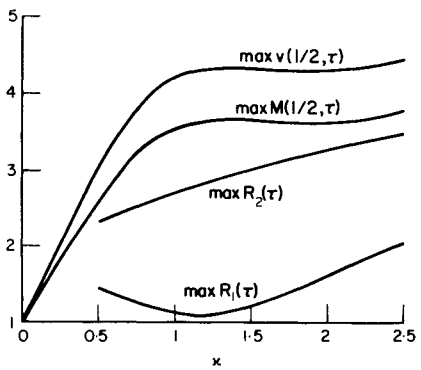

FIG. 10. Effect of mass parameter $\varkappa$. Case No. 30, $a_1 = 0$, $a_2 = 20$, $\alpha = 0{\cdot}02$.

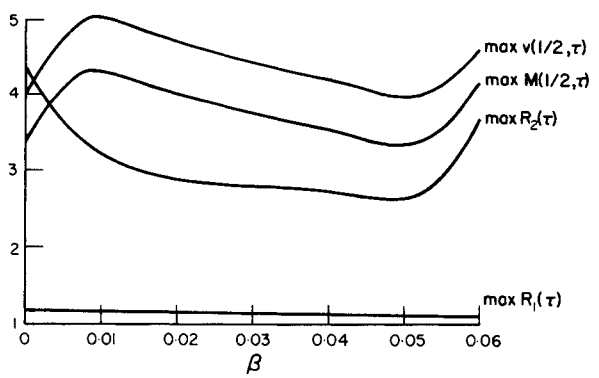

FIG. 11. Effect of sprung frequency parameters β_i. Case No. 30, $a_1 = 0$, $a_2 = 20$, $\alpha = 0{\cdot}02$.

If the parameter $\varkappa_i$ (17) (in the range $0{\cdot}025 \leq \varkappa_i \leq 0{\cdot}1$) is increasing the dynamic stresses of the beam are slightly rising up to $\varkappa_i \approx 0{\cdot}05$. Then they are kept constant approximately. The effect of the parameter b_2 (23) is similar to that one as shown in the Fig. 13

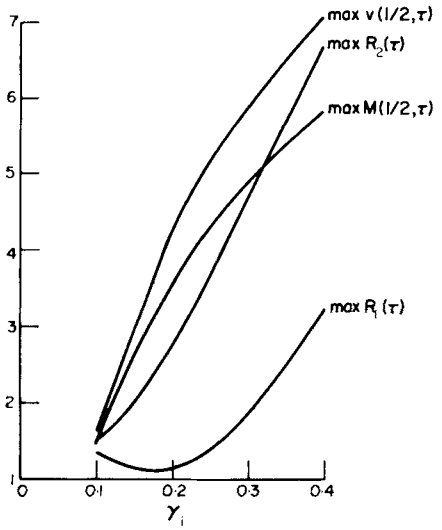

FIG. 12. Effect of unsprung frequency parameters γ_i. Case No. 30, $a_1 = 0$, $a_2 = 20$, $\alpha = 0{\cdot}02$.

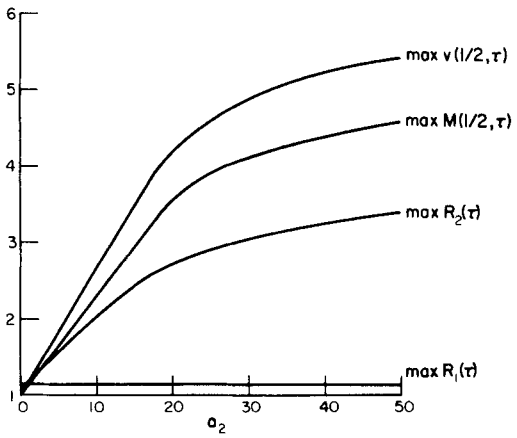

FIG. 13. Effect of depth parameter a_2. Case No. 30, $a_1 = 0$, $b_2 = 0{\cdot}02$, $\alpha = 0{\cdot}02$.

TABLE 1. A SET OF INPUT PARAMETERS

1	No. of case	30	13	λ	0·2	25	B_1	0
2	v_{10}	10	14	α	0·02	26	B_2	−1
3	v_{20}	10	15	β_1	0·04	27	d	1
4	v_{30}	10	16	β_2	0·04	28	d_1	0·5
5	φ_0	0	17	γ_1	0·2	29	ϑ	0·5
6	$\dot{v}_{10}$	0	18	γ_2	0·2	30	ϑ_1	0·5
7	$\dot{v}_{20}$	0	19	a_1	0	31	ϑ_2	0·5
8	$\dot{v}_{30}$	0	20	a_2	20	32	h_1	0·001
9	$\dot{\varphi}_0$	0	21	b_1	0·02	33	h_2	0·0001
10	$\varkappa$	1	22	b_2	0·02	34	N	10
11	$\varkappa_1$	0·05	23	A_1	0·5	35	s	3
12	$\varkappa_2$	0·05	24	A_2	0·5			

TABLE 2. EFFECT OF INTEGRATION STEP LENGTH AND OF NUMBER s OF EQUATIONS (case No. 30)

h_1	0·001		0·0005	
h_2	0·0001		0·0001	
s	1	3	1	3
$\tau[\max M(\frac{1}{2}, \tau)]$	1·5710999	1·5710999	1·5710999	1·5715999
$\max M(\frac{1}{2}, \tau)$	3·5583133	3·5504918	3·5583731	3·5603028
$\tau[\max v(\frac{1}{2}, \tau)]$	1·5720999	1·5720999	1·5725999	1·5725999
$\max v(\frac{1}{2}, \tau)$	4·1934544	4·2011628	4·1948825	4·2038006
$\tau[\max R_1(\tau)]$	0·0220000	0·0220000	0·0220000	0·0220000
$\max R_1(\tau)$	1·1385666	1·1384909	1·1385666	1·1384909
$\tau[\max R_2(\tau)]$	0·0209000	0·0209000	0·0209000	0·0209000
$\max R_2(\tau)$	2·7198116	2·7198118	2·7198118	2·7198118

(for $0 \leq b_2 \leq 0{\cdot}04$, case No. 30). The parameter λ (18) expressing the rotatory characteristics of the sprung mass has in the range $0{\cdot}1 \leqq \lambda \leqq 0{\cdot}3$ no effect on the maxima of functions $M(1/2, \tau)$ and $v(1/2, \tau)$. The effect of the initial conditions (42) was also studied. In comparison with the case when impact occurs the dynamic effect of the initial conditions just mentioned is small for the case of no unevenness ($a_i = 0$).

4. CONCLUSIONS

The paper presents a discussion concerning the vibrations of a simple beam carrying an elastic layer forced by a moving system of four degrees of freedom. There are supposed irregularities on the travel surface, so that impacts between the moving system and the beam may occur. The linearized Hertz's contact law is supposed to hold true and also the loss of contact between the two solids can take place. The mathematical formulation results in a system of five differential equations with variable coefficients that is solved numerically by the method of Runge–Kutta–Nyström using the computer Ural 2.

In technical practice the described system is an idealization of the dynamic effects of a moving vehicle crossing a bridge. The theory was verified by field tests carried out on four railway bridges under the action of moving car with flat wheels. The experimental results and the comparison between the theoretical and experimental deflections and bending moments of the four bridges mentioned are described in detail in [12].

The most important results of present investigations concerning the effect of an isolated unevenness (flat wheel of a car) are as follows:

1. The dynamic effects have their maximum at the low velocity (in practice around 25–50 km/hr).

2. The dynamic effects are rising with increasing vehicle mass but unsprung masses have only a smaller effect.

3. If the stiffness of the roadway is increasing the beam stresses attain higher values as well.

4. The dynamic stresses of the beam increase almost in direct proportion to the depth of an unevenness.

5. The effect of track or wheel irregularities is much greater than the effect of initial conditions of the vehicle.

REFERENCES

[1] S. P. TIMOSHENKO and D. H. YOUNG, *Vibration Problems in Engineering*, 3rd edition. Van Nostrand (1955).
[2] C. E. INGLIS, *A Mathematical Treatise on Vibrations in Railway Bridges*. Cambridge University Press (1934).
[3] V. KOLOUŠEK, *Calcul des efforts dynamiques dans les ossatures rigides*. Dunod (1959).
[4] A. HILLERBORG, *Dynamic Influences of Smoothly Running Loads on Simply Supported Girders*. Kungl. Tekniska Högskolan, Stockholm (1951).
[5] J. M. BIGGS, H. S. SUER and J. M. LOUW, Vibration of simple-span highway bridges. *Trans. Am. Soc. civ. Engrs* **124**, 291–318 (1959).
[6] T. P. TUNG, L. E. GOODMAN, T. Y. CHEN and N. M. NEWMARK, Highway-bridge impact problems. *Highw. Res. Bull.* **124**, 111–134 (1956).
[7] L. FRÝBA, Dynamik des Balkens mit federnder Schicht veränderlicher Steifigkeit unter der Wirkung eines bewegten Systems. *Proc. 11th int. Congr. appl. Mech.* Munich 1964, pp. 245–251, Springer (1966).
[8] R. K. WEN, Dynamic response of beams traversed by two-axle loads. *J. Engng Mech. Div. Am. Soc. civ. Engrs* **86**, 91–111 (1960).
[9] W. GOLDSMITH, *Impact. The Theory and Physical Behaviour of Colliding Solids*. Arnold (1960).
[10] L. FRÝBA, Schwingungen des unendlichen, federnd gebetteten Balkens unter der Wirkung eines unrunden Rades. *Z. angew. Math. Mech.* **40**, 170–184 (1960).
[11] L. COLLATZ, *Numerische Behandlung von Differentialgleichungen*, 2nd edition. Springer (1955).
[12] L. FRÝBA, The dynamic influence of wheel flats on railway bridges. *Mon. Bull. int. Rly Congr. Ass.* **44**, 477–512 (1967).

(*Received* 26 *February* 1968; *revised* 29 *April* 1968)

Абстракт—В работе решается колебание шарнирно опертой балки с упругим слоем и с неровностями рабочей поверхности мостовой. Колебания вынужденны ударами движущейся системы с четырмя степенями свободы, что в технической практике представляет движение двухосового состава по мосте. Математическая формулировка приводит к системе пяти дифференциальных уравнений с переменными козффициентами, решение которой выполнено на вычислительной машине. Анализ влияния некоторых безразмерных параметров приводит к нескольким важнейшим результатам, напр. найбольшие дниамические напряжения балки вызванные изолированной неровностей возникают при низких скоростях движения.